Pump-Controlled Plasmonic Random Lasers from Dye-Doped Nematic Liquid Crystals with TiN Nanoparticles in Non-Oriented Cells

Yuan Wan and Luogen Deng * ![ORCID]

School of Physics, Beijing Institute of Technology, Beijing 100081, China; wan_yuan_meng@163.com
* Correspondence: luogen@bit.edu.cn

Abstract: Manipulation of the performance of the random lasers from dye-doped nematic liquid crystals with TiN nanoparticles in non-oriented cells is studied. The experimental results show that the introduction of TiN nanoparticles into dye-doped nematic liquid crystals significantly reduces the threshold of random lasing due to the localized surface plasmon resonance of TiN nanoparticles. The emission spectrum of random lasers can be controlled by the shape of the pump spot. The threshold of random lasers increases with the decrease of the length of pump stripe. In order to obtain the emission spectrum with fine discrete sharp peaks, the narrow pump stripe is more effective than the circular pump spot. When the pump area is more like a circle, the emission spectrum is more like an amplified spontaneous emission. The underlying mechanisms of these phenomena are discussed in detail. This study provides a promising platform for designing the high-quality and low-threshold random lasers which can be controlled by the shape of the pump spot.

Keywords: random lasers; TiN nanoparticles; localized surface plasmon resonance; multiple scattering

1. Introduction

Conventional laser is usually formed by three basic elements: a gain medium, an exciting source, and an optical resonant cavity. However, since Letokhov [1] theoretically proposed in 1968 that the optical feedback of stimulated emission can be provided by scatterers, a new avenue for the realization of lasers without cavity has been opened. Random lasers, whose optical feedback is the multiple scattering caused by random fluctuations of the dielectric constant in space, have attracted widespread attentions due to their unique physical mechanisms and potential applications [2–6]. Generally, the generation of random lasers must satisfy two conditions: (i) light is amplified by the stimulated emission and the feedback comes from the multiple scattering, and (ii) there is an energy threshold which is defined by the sharp narrowing of the spectrum and the sharp increase of the peak intensity as the pump energy increases. When the pump energy exceeds the threshold, the total gain overcomes the total loss in the random system, which results in the occurrence of random lasers. In the past few decades, a wide range of materials, such as semiconductor [7], π-conjugated [8], human tissues [9], quantum dots [10], metallic nanoparticles [11,12], polymers [13], and liquid crystals (LCs) [14–16] have been used to realize random lasers. Metal nanoparticles, such as gold (Au) nanoparticles and silver (Ag) nanoparticles are often used to enhance the performances of random lasers [11,12,17–20]. For example, Dice et al. [17] reported in 2005 that the random lasers formed by suspending Ag nanoparticles in the laser dye solution. In 2006, Popov et al. [18] studied the dye-doped polymer film random lasers enhanced by Au nanoparticles. In 2016, Ye et al. [19] investigated the influence of Ag nanoparticles on random lasers from dye-doped nematic liquid crystals. In 2019, the recyclable random lasers assisted by metal nanoparticles in DCM dye doped polyvinyl alcohol (DCM-PVA) thin films are studied [20].

Nematic liquid crystals are one of ideal materials for fabricating random lasers because of its unique optical characteristics. The scattering intensity of nematic liquid crystals is very strong in the visible region, which is about 10^6 times larger than that of the isotropic liquid [21]. Moreover, the director of nematic liquid crystals is easily modulated by the external stimuli including the electric field, magnetic field, temperature, and light [22–25]. Recently, we reported a plasmonic random laser of dye-doped nematic liquid crystals with TiN nanoparticles in capillary tubes. Advantages of this random laser enhanced by localized surface plasmon resonance (LSPR) of TiN nanoparticles have been discussed in our article [26]. However, the manipulation of the random laser emission from dye-doped nematic liquid crystals with TiN nanoparticles (NPDDNLC) in non-oriented cells has not been studied.

Over the past few decades, plenty of methods have been proposed for controlling the performance of random lasers [27–33]. Some deals with adjusting the scatterers, others depend on controlling the gain. However, these methods either change the random structures or use different samples. This needs a complex manufacturing process, which limits the actual application of random lasers. For most applications, active manipulation of random lasers is more desired. Among these methods, the partial pump control, which can be operated in a single random sample, are simpler. Therefore, we adopt this method to control the performance of random lasers from dye-doped nematic liquid crystals with TiN nanoparticles in non-oriented cells.

In this work, we achieve experimentally the control of the high-quality and low-threshold random lasers by tuning the shape of the pump spot. The experimental results show that the introduction of TiN nanoparticles into dye-doped nematic liquid crystals makes the threshold of random lasers be reduced tenfold owing to the localized surface plasmon resonance of TiN nanoparticles. The narrow pump stripe is more effective than the circular pump spot for the realization of coherent random lasers with discrete sharp peaks on the emission spectrum. When the pump area is more like a circle, the emission spectrum is more like an amplified spontaneous emission. The potential reasons for these phenomena are discussed.

2. Materials and Methods

The experimental materials used in this experiment include nematic liquid crystals (P0616A, from slichem), TiN nanoparticles (diameter d = 40 nm, from DK nano), and the laser dye DCM (from Exciton). The sample making process is as follows: the TiN nanoparticles and DCM are dispersed in nematic liquid crystals with the density of 5.314×10^{11} /mL and 0.3 wt%, respectively. Then, the mixture is stirred for one hour, and the ultrasonic process is performed to ensure the homogeneous mixing. The liquid crystal cell fabricated by two glass slides with non-oriented is filled by the mixture due to the capillary effect. The gap of the liquid crystal cell is 20 μm.

Figure 1 shows the schematic diagram of the experimental setup. The sample is optically pumped by a second harmonic of a Q-switched Nd: YAG laser (λ = 532 nm, 10 Hz in repetition rate, and 8 ns in pulse duration). The pump energy can be adjusted by the energy attenuator formed by a half-wave plate and a polarizer. Then, the pump light is split into two sub-beams with the same energy by a neutral beam splitter. One beam is recorded by an energy meter as a reference light. The other beam is focused by a cylindrical lens and adjusted by a slit before irradiating the sample. The polarization of the pump beam is parallel to the *x*-axis as shown in Figure 1. The excited stripe is 1 cm of length and 0.2 mm of width when there are no special instructions. The single-shot emission spectrum of the sample is measured by a fiber spectrometer with the spectral resolution of 0.13 nm.
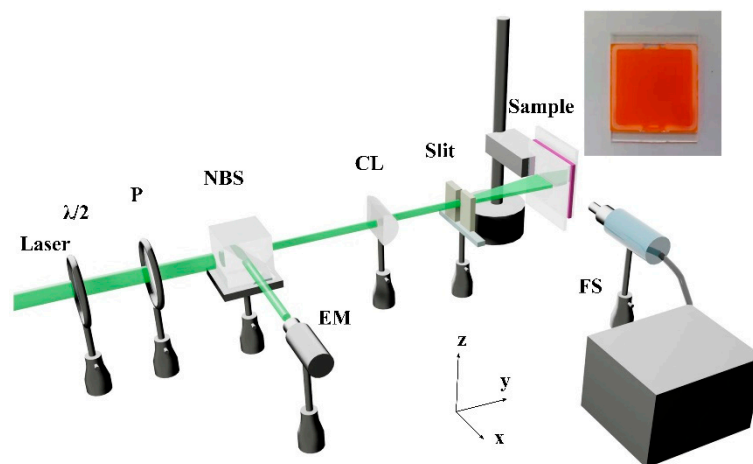
Figure 1. The schematic diagram of the experimental setup. The inset is the optical photograph of the sample. $\lambda/2$, P, NBS, CL, EM, and FS express the half-wave plate, polarizer, neutral beam splitter, cylindrical lens (focal length of 10 cm), energy meter, and fiber spectrometer, respectively.

3. Results

Figure 2a shows the evolution of the emission spectrum of the NPDDNLC sample as the pump energy density increases from 0.135 mJ/cm^2 to 0.39 mJ/cm^2. The pump energy density is defined as the ratio of the pump energy to the pump area. When the pump energy density is low, the emission spectrum is a broad spontaneous emission with the full width at half maximum (FWHM) of about 35 nm. As the pump energy increases, some discrete sharp peaks suddenly emerge on the top of the spontaneous emission spectrum. The FWHM of the discrete sharp peaks is about 0.3 nm, which is more than 100 times smaller than the FWHM of the spontaneous emission. This indicates the occurrence of coherent random lasers. When the pump energy density further increases, more discrete sharp peaks appear on the top of the spontaneous emission spectrum, and the peak intensity of the sharp peaks increases sharply. The peak intensity and FWHM of the emission spectrum of the NPDDNLC sample as a function of the pump energy density are shown in Figure 2b. The peak intensity of the emission spectrum increases slowly as the pump energy density increases to 0.2 mJ/cm^2. However, when the pump energy density is larger than 0.2 mJ/cm^2, the peak intensity of the emission spectrum increases dramatically. The FWHM of the emission spectrum narrows slowly as the pump energy density increases to 0.2 mJ/cm^2. However, when the pump energy density exceeds 0.2 mJ/cm^2, the FWHM of the emission spectrum narrows sharply to about 0.3 nm. Therefore, we obtain that the pump threshold, defined by the sharp narrowing of the emission spectrum and the slope changing of the peak intensity as the pump energy density increases, is about 0.2 mJ/cm^2, which is much lower than that in the references [10,34–36].
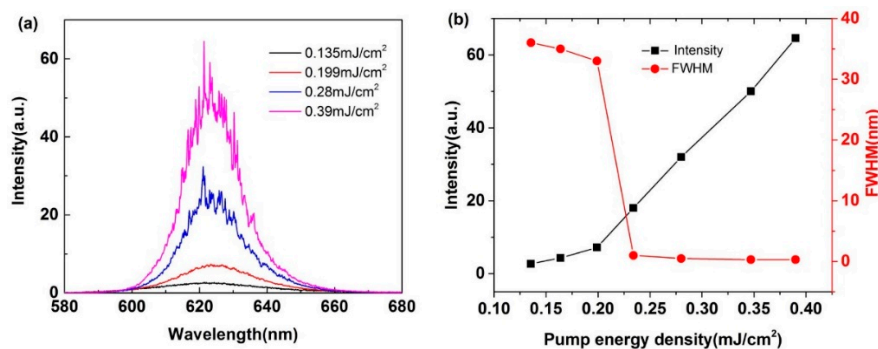

Figure 2. (**a**) Evolution of the emission spectrum of the NPDDNLC sample as a function of the pump energy density. (**b**) The peak intensity and FWHM of the emission spectrum of the NPDDNLC sample as a function of the pump energy density.

For investigating the influence of the TiN nanoparticles on the performance of random lasers of the NPDDNLC sample, we also studied the emission spectrum of the dye-doped nematic liquid crystal (DDNLC) sample at different pump energy densities as shown in Figure 3a. Similar to Figure 2a, some discrete sharp peaks can be observed on the top of the spontaneous emission spectrum. However, it is worth noting that the emission spectrum of the DDNLC sample as a function of the pump energy density has some different characteristics compared to that of the NPDDNLC sample shown in Figure 2a. Although, the pump energy density in the DDNLC sample is much larger than that in the NPDDNLC sample, the number of the discrete sharp peaks of the emission spectrum of the DDNLC sample is much less than that of the NPDDNLC sample. The discrete sharp peaks of the emission spectrum of the DDNLC sample is weaker and the amplitude of the spontaneous emission is larger than that of the NPDDNLC sample. Figure 3b shows the peak intensity and FWHM of the emission spectrum of the DDNLC sample as a function of the pump energy density. Similar to Figure 2b, the peak intensity of the emission spectrum increases distinctly and FWHM of the emission spectrum narrows sharply when the pump energy density exceeds a given value. However, the pump threshold of the DDNLC sample is about 2.0 mJ/cm^2, which is 10 times larger than the pump threshold of the NPDDNLC sample. In addition, the slope efficiency of the NPDDNLC sample, defined as the increase amplitude of the peak intensity of emission spectrum for unit pump energy density, is about 10 times larger than that of the DDNLC sample, which means that the conversion rate of the pump energy into lasing is increased dramatically by adding the TiN nanoparticles into DDNLC.
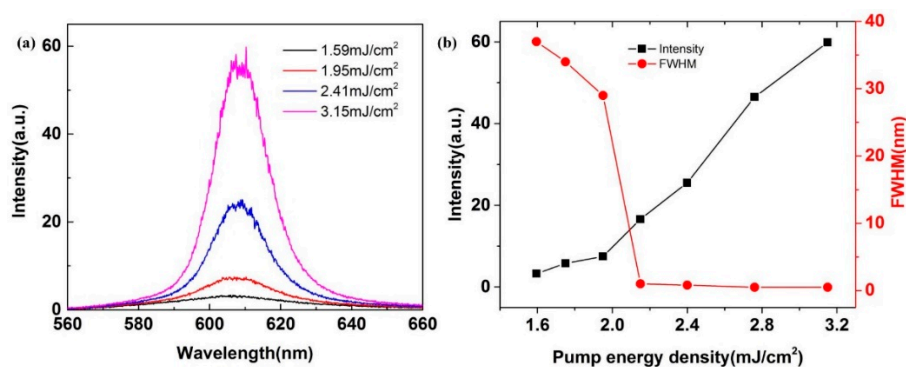

Figure 3. (**a**) Evolution of the emission spectrum from the DDNLC sample as a function of the pump energy density. (**b**) The peak intensity and FWHM of the emission spectrum from the DDNLC sample as a function of the pump energy density.

Figure 4a shows the texture of the sample measured by an orthogonal polarizing microscope. Figure 4b shows the schematic illustration of the random laser of the NPDDNLC sample. The non-oriented cells result in the non-uniform alignment of NLC molecules. As shown in Figure 4a, the NLC molecules are self-assembled into many micro-domains and the micro-domain possesses a residual birefringence [37,38]. The orientation of the micro-domains near the inner surfaces of the cell is parallel to the surfaces of the cell due to the weak anchoring force from the inner surfaces of the cell. The orientation of the micro-domains away from the surfaces of the cell is chaotic. Because of the long-range fluctuations of the micro-domain director, the dielectric tensor of NLC molecules is different between the adjacent micro-domains, then the spatial refractive index is not uniform in the cell [39]. The light is confined in the cell and has a longer dwelling time in the cell because of the multiple scattering of micro-domains. This is also the reason why random lasers can occur in the DDNLC samples. In addition, the introduction of TiN nanoparticles into the DDNLC solution can enhance the emission spectrum by two mechanisms. On the one hand, the electromagnetic field around TiN nanoparticles is enhanced by the LSPR of the TiN nanoparticles. This effectively increases the pump absorption and the fluorescence amplification efficiency of the DCM molecules around TiN nanoparticles. On the other hand, the scattering strength of the sample is enhanced by adding TiN

nanoparticles into the sample. This makes that the dwelling time of the light in the sample is increased markedly. When the gain exceeds the loss, the random laser occurs.
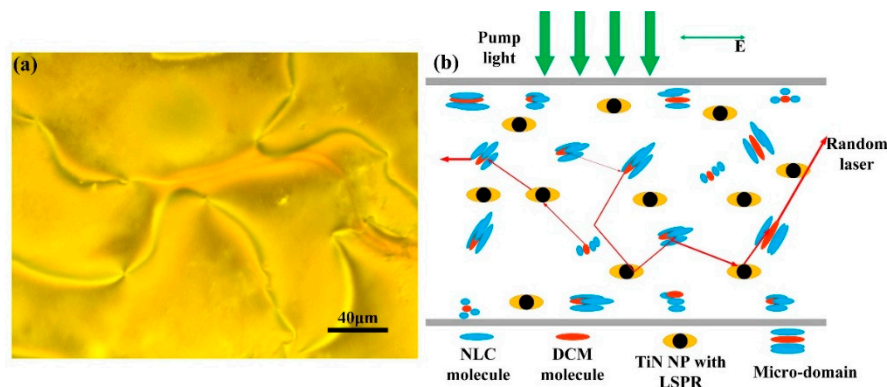

Figure 4. (**a**) The texture of the sample measured by an orthogonal polarizing microscope. (**b**) Schematic illustration of the random laser of the NPDDNLC sample.

In order to study the influence of the length of pump stripe on the emission spectrum, an adjustable slit is added in front of the sample as shown in Figure 1, which can change the length of pump stripe illuminated on the sample. Figure 5a shows the emission spectrum of the NPDDNLC sample as a function of the length of pump stripe, when the pump energy density is 0.52 mJ/cm^2. The emission intensity decreases with decreasing the length of pump stripe from 10 mm to 2 mm. In addition, the number of the discrete sharp peaks decreases markedly with the decrease of the length of pump stripe. As we can see in Figure 5a, the discrete sharp peaks disappear when the length of pump stripe decreases to be less than 4 mm. This is because the gain length of the photons emitted from the dye molecules reduces with the decrease of the length of pump stripe. The effective region of the system [40], defined as the pump region plus the absorption length, decreases with the decrease of the length of pump stripe, which makes the reduction of the random laser modes in the sample. When the length of pump stripe decreases to a given value, the discrete sharp peaks will disappear due to the fact that the gain is smaller than the loss. It also means that the pump energy is lower than the threshold. Figure 5b shows the pump threshold of the NPDDNLC sample as a function of the length of pump stripe. The pump threshold increases with the decrease of the length of pump stripe. When the length of pump stripe is longer than 6 mm, the pump energy density (0.52 mJ/cm^2) is larger than the pump threshold. Therefore, the discrete sharp peaks can be observed. When the length of pump stripe is shorter than 4 mm, the pump energy density is lower than the pump threshold. Therefore, the random laser action cannot occur.
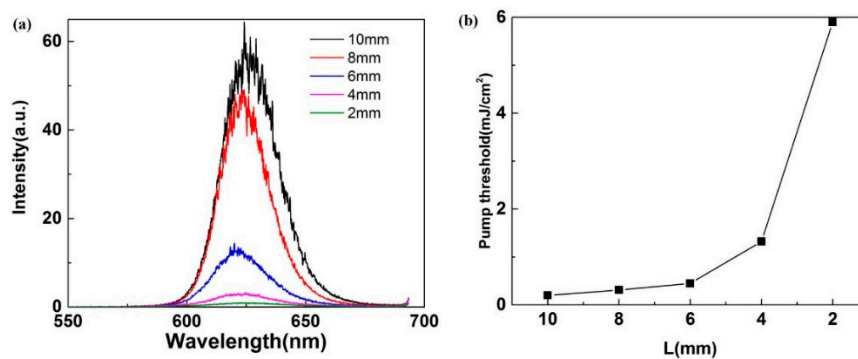

Figure 5. (**a**) The emission spectrum of the NPDDNLC sample as a function of the length (L) of pump stripe, when the pump energy density is 0.52 mJ/cm^2. (**b**) The pump threshold of the NPDDNLC sample as a function of the length of pump stripe.

Here, the influence of the width of pump area on the emission spectrum is studied. In this process, the silt is removed. The pump area is an ellipse whose length (i.e., the length of the ellipse's long-axis) is fixed (about 10 mm), and its width (i.e., the length of the ellipse's short-axis) can be tuned by changing the distance between the sample and the cylindrical lens. Figure 6a shows the emission spectrum of the NPDDNLC sample at different widths of pump area when the pump energy density is about 0.54 mJ/cm². According to common sense, the number and the intensity of the discrete sharp peaks should increase with the increase of the pump area because of the increase of the effective region of the system. However, according to our experimental data, the number and the intensity of the observed discrete sharp peaks decrease with the increase of the width of pump area. As we can see in Figure 6a, when the width is shorter than 2 mm, the discrete sharp peaks can be observed clearly. When the width of pump area increases to be larger than 3 mm, the discrete sharp peaks can be observed poorly. Further increasing the width of pump area to be longer than 6 mm, it is difficult to see the discrete sharp peaks. This can be explained by two different reasons: (i) when the width of pump area increases, the light emitted from dye molecules can be amplified not only along the direction of the long side of the pump area, but also along the other directions of the pump area. The number of local modes increases with the increase of the pump area. However, the gain efficiency of the DCM molecules is limited when the pump energy density is fixed. Therefore, the fierce competition between different modes exists. In addition, the emission spectrum along other directions is not collected because the experimental data are collected along the direction of the long side of the pump area. When the gain is occupied by the modes along other directions, the intensity of the lasing modes along the direction of the long side of the pump area decreases, even these modes cannot be excited. (ii) The lasing threshold of different local modes is very similar because the random system used in our experiment is a weak scattering system [40]. When the pump area is small, fewer modes can be excited, and the distance between two adjacent lasing modes is big enough to let us observe clearly some discrete sharp peaks on the emission spectrum. When the width of pump area increases, the lasing threshold of the sample decreases due to the fact that a bigger gain area results in more modes which can be stimulated simultaneously [29]. The resonant modes are coupled to each other and their spectrum will overlap [41]. Therefore, the lasing modes cannot be distinguished. In this case, the emission spectrum is smooth and its characteristics are more like an amplified spontaneous emission (ASE).
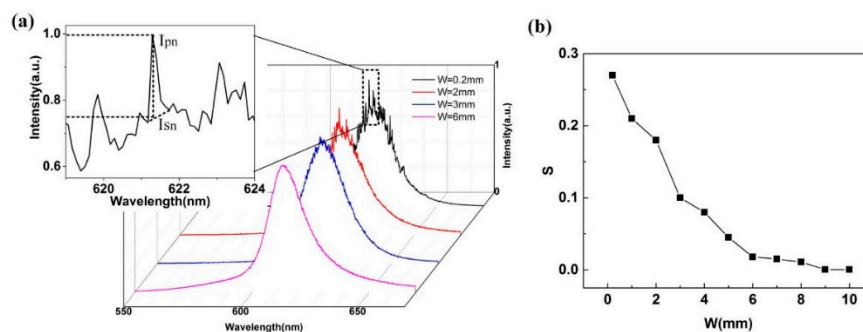

Figure 6. (**a**) The emission spectrum of the NPDDNLC sample at different widths (W) of pump area. The inset shows the enlarged view of the corresponding rectangle area. (**b**) The sharpness of the laser modes as a function of the width of pump area. The length of pump area is 10 mm and the pump energy density is about 0.54 mJ/cm².

The visibility of laser modes can be evaluated by the sharpness (*S*) of laser modes. The sharpness of laser modes can be expressed as:

$$S = \frac{I_{pn} - I_{sn}}{I_{pn}} \tag{1}$$

where I_{pn} expresses the peak intensity of the nth laser mode, I_{sn} expresses the intensity of the amplified spontaneous emission (ASE) curve of the nth laser mode as shown in the inset of Figure 6a. When the

value of the sharpness S approaches 1, the laser mode is very good and sharp. When the value of the sharpness S approaches 0, the emission spectrum is smooth. Figure 6b shows the sharpness of laser modes as a function of the width of pump area. As we can see in Figure 6b, the sharpness of laser modes decreases with the increase of the width of pump area. When the width of pump area exceeds 6 mm, the sharpness S is close to 0.

For comparison, the emission spectrum of the NPDDNLC sample is studied when the pump area is a circular spot. In this process, the cylindrical lens shown in Figure 1 is replaced by a convex lens with the focal length of 10 cm, which can focus the pump light to be a circular spot. The diameter of pump spot can be tuned by changing the distance between the sample and the convex lens. Figure 7a shows the emission spectrum of the NPDDNLC sample at different pump energies, when the diameter (D) of pump area is 10 mm. Unlike the emission spectrum shown in Figure 2a, the discrete sharp peaks cannot be observed clearly on the top of the emission spectrum shown in Figure 7a when the pump energy density increases from 0.098 mJ/cm^2 to 0.543 mJ/cm^2. The emission spectrum is more like an ASE spectrum. The inset of the Figure 7a shows the peak intensity of the corresponding emission spectrum as a function of the pump energy density. The peak intensity of the emission spectrum increases near linearly with the increase of the pump energy density. There is no obvious lasing threshold as shown in the inset of the Figure 7a. This further proves that the emission spectrum is more like an ASE spectrum. Figure 7b shows the emission spectrum of the NPDDNLC sample as a function of the diameter of pump area, when the pump energy density is 0.57 mJ/cm^2. The inset of the Figure 7b shows the peak intensity of the corresponding emission spectrum as a function of the diameter of pump area. The intensity of emission spectrum decreases with the diameter of pump area decreases from 10 mm to less than 1 mm. However, the obvious discrete sharp peaks are not observed during this process. From what has been discussed above, we may safely draw the conclusion that the random lasing modes and the lasing threshold can be controlled by the external pumping setup. The transition between the coherent random laser and the amplified spontaneous emission can be operated by changing the shape of the pump area. In addition, the stripe-shape of the pump area is more effective than the circle-shape of the pump area for the occurrence of coherent random lasers.
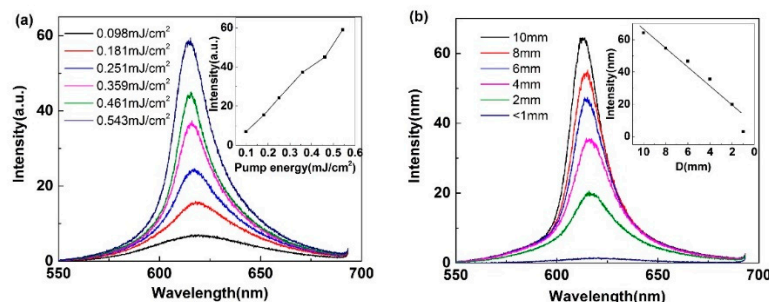

Figure 7. The emission spectrum of the NPDDNLC sample when the pump area is a circle spot. (**a**) The emission spectrum of the NPDDNLC sample at different pump energy densities, when the diameter (D) of pump area is 10 mm. Inset shows the peak intensity of the corresponding emission spectrum as a function of the pump energy density. (**b**) The emission spectrum of the NPDDNLC sample as a function of the diameter of pump area, when the pump energy density is 0.57 mJ/cm^2. Inset shows the peak intensity of the corresponding emission spectrum as a function of the diameter of pump area.

4. Conclusions

In conclusion, it has been demonstrated experimentally that high-quality and low-threshold random lasers formed by the dye-doped nematic liquid crystals with TiN nanoparticles in non-oriented cells can be controlled by the shape of the pump spot. The results show that the threshold of the NPDDNLC sample is about 10 times lower than that of the DDNLC sample because of the LSPR of TiN nanoparticles. The threshold of the random laser from the NPDDNLC sample increases with the

decrease of the length of pump stripe. The number of discrete sharp peaks observed on the top of the emission spectrum decreases with the increase of the width of the pump stripe. When the width of the pump stripe is larger than 6 mm, the emission spectrum of the NPDDNLC sample is more like an ASE spectrum. For comparison, we also studied the evolution of the emission spectra of the NPDDNLC samples with the diameter of the circular pump spot. We can draw the conclusion that the narrow pump stripe is more effective than the circular pump spot for the generation of coherent random lasers with discrete sharp peaks. Our study provides an effective way for the realization of the high-quality and low-threshold random lasers of which the characteristics can be controlled by the shape of the pump spot.

Author Contributions: Contributed to the main idea and the methodology of the research, L.D. and Y.W.; Wrote the original manuscript, Y.W.; Reviewed the manuscript and provided valuable suggestions to further refine it, L.D. All authors have read and agreed to the published version of the manuscript.

Conflicts of Interest: The authors declare no conflict of interest.

References

1. Letokhov, V.S. Generation of light by a scattering medium with negative resonance absorption. *Sov. Phys. JETP* **1968**, *26*, 835.
2. Redding, B.; Choma, M.A.; Cao, H. Speckle-free laser imaging using random laser illumination. *Nat. Photonics* **2012**, *6*, 355–359. [CrossRef] [PubMed]
3. Ismail, W.Z.W.; Liu, G.Z.; Zhang, K.; Goldys, E.M.; Dawes, J.M. Dopamine sensing and measurement using threshold and spectral measurements in random lasers. *Opt. Express* **2015**, *24*, A85–A91. [CrossRef]
4. Uppu, R.; Mujumdar, S. Lévy exponents as universal identifiers of threshold and criticality in random lasers. *Phys. Rev. A* **2014**, *90*, 025801. [CrossRef]
5. Wiersma, D. The physics and applications of random laser. *Nat. Phys.* **2008**, *4*, 359–367. [CrossRef]
6. Shi, X.Y.; Liao, Y.M.; Lin, H.Y.; Tsao, P.W.; Wu, M.J.; Lin, S.Y.; Hu, H.H.; Wang, Z.N.; Lin, T.Y.; Lai, Y.C.; et al. Dissolvable and recyclable random lasers. *ACS Nano* **2017**, *11*, 7600–7607. [CrossRef]
7. Cao, H.; Zhao, Y.G.; Ho, S.T.; Seeling, E.W.; Wang, Q.H.; Chang, R.P. Random laser action in semiconductor powder. *Phys. Rev. Lett.* **1999**, *82*, 2278–2281. [CrossRef]
8. Frolov, S.V.; Vardeny, Z.V.; Yoshino, K.; Zakhidov, A.; Baughman, R.H. Stimulated emission in high-gain organic media. *Phys. Rev. B* **1999**, *59*, R5284. [CrossRef]
9. Polson, R.C.; Vardeny, Z.V. Random lasing in human tissues. *Appl. Phys. Lett.* **2004**, *85*, 1289–1291. [CrossRef]
10. Cao, M.X.; Zhang, Y.T.; Song, X.X.; Che, Y.L.; Zhang, H.T.; Dai, H.T.; Zhang, G.Z.; Yao, J.Q. Random lasing in a colloidal quantum dot-doped disordered polymer. *Opt. Express* **2016**, *24*, 9325–9331. [CrossRef]
11. Chang, Q.; Shi, X.Y.; Liu, X.; Tong, J.H.; Liu, D.H.; Wang, Z.N. Broadband plasmonic silver nanoflowers for high-performance random lasing covering visible region. *Nanophotonics* **2017**, *6*, 1151–1160. [CrossRef]
12. Wang, L.; Wan, Y.; Shi, L.J.; Zhong, H.Z.; Deng, L.G. Electrically controllable plasmonic enhanced coherent random lasing from dye-doped nematic liquid crystals containing Au nanoparticles. *Opt. Express* **2016**, *24*, 17593–17602. [CrossRef] [PubMed]
13. Meng, X.G.; Fujita, K.; Zong, Y.H.; Murai, S.; Tanaka, K. Random lasers with coherent feedback from highly transparent polymer films embedded with silver nanoparticles. *Appl. Phys. Lett.* **2008**, *92*, 201112. [CrossRef]
14. Ferjani, S.; Barna, V.; De Luca, A.; Versace, C.; Scaramuzza, N.; Bartolino, R.; Strangi, G. Thermal behavior of random lasing in dye doped nematic liquid crystals. *Appl. Phys. Lett.* **2006**, *89*, 121109. [CrossRef]
15. Bian, H.T.; Yao, F.F.; Liu, H. Optically controlled random lasing based on photothermal effect in dye-doped nematic liquid crystals. *Liq. Cryst.* **2014**, *41*, 1436–1441. [CrossRef]
16. Li, L.W.; Deng, L.G. Random lasing from dye-doped chiral nematic liquid crystals in oriented and non-oriented cells. *Eur. Phys. J. B* **2013**, *86*, 112. [CrossRef]
17. Dice, G.D.; Mujumdar, S.; Elezzabi, A.Y. Plasmonically enhanced diffusive and subdiffusive metal nanoparticle-dye random laser. *Appl. Phys. Lett.* **2005**, *86*, 131105. [CrossRef]
18. Popov, O.; Zilbershtein, A.; Davidov, D. Random lasing from dye-gold nanoparticles in polymer films: Enhanced gain at the surface-plasmon-resonance wavelength. *Appl. Phys. Lett.* **2006**, *89*, 436. [CrossRef]

19. Ye, L.H.; Liu, B.; Li, F.J.; Feng, Y.Y.; Cui, Y.P.; Lu, Y.Q. The influence of Ag nanoparticles on random laser from dye-doped nematic liquid crystals. *Laser Phys. Lett.* **2016**, *13*, 105001. [CrossRef]

20. Wan, Y.; Deng, L.G. Recyclable coherent random lasers assisted by plasmonic nanoparticles in DCM-PVA thin films. *Opt. Express* **2019**, *27*, 27103–27111. [CrossRef]

21. De Gennes, P.G.; Prost, J. *The Physics of Liquid Crystals*; Oxford University Press Inc.: New York, NY, USA, 1993; p. 139.

22. Lee, C.R.; Lin, S.H.; Guo, J.W. Electrically and thermally controllable nanoparticle random laser in a well-aligned dyedoped liquid crystal cell. *Opt. Mater. Express* **2015**, *5*, 1469–1481. [CrossRef]

23. Wiersma, D.S.; Cavalieri, S. A temperature-tunable random laser. *Nature* **2001**, *414*, 708–709. [CrossRef] [PubMed]

24. Lee, C.R.; Lin, S.H.; Guo, C.H.; Chang, S.H.; Mo, T.S.; Chu, S.C. All-optically controllable random laser based on a dye-doped polymer-dispersed liquid crystal with nano-sized droplets. *Opt. Express* **2010**, *18*, 2406–2412. [CrossRef] [PubMed]

25. Perumbilavil, S.; Kauranen, M.; Assanto, G. Magnetic steering of beam-confined random laser in liquid crystals. *Appl. Phys. Lett.* **2018**, *113*, 121107. [CrossRef]

26. Wan, Y.; An, Y.S.; Deng, L.G. Plasmonic enhanced low-threshold random lasing from dye-doped nematic liquid crystals with TiN nanoparticles in capillary tubes. *Sci. Rep.* **2017**, *7*, 16185. [CrossRef] [PubMed]

27. Ning, S.Y.; Wu, Z.X.; Dong, H.; Ma, L.; Jiao, B.; Ding, L.; Ding, L.P.; Zhang, F.H. The enhanced random lasing from dye-doped polymer films with different-sized silver nanoparticles. *Org. Electron.* **2016**, *30*, 165–170. [CrossRef]

28. Ye, L.H.; Liu, B.; Zhao, C.; Wang, Y.; Cui, Y.P.; Lu, Y.Q. The electrically and magnetically controllable random laser from dye-doped liquid crystals. *J. Appl. Phys.* **2014**, *116*, 053103. [CrossRef]

29. Andreasen, J.; Cao, H. Spectral behavior of partially pumped weakly scattering random lasers. *Opt. Express* **2011**, *9*, 3418–3433. [CrossRef]

30. Meng, X.G.; Fujita, K.; Murai, S.; Matoba, T.; Tanaka, K. Plasmonically Controlled Lasing Resonance with Metallic-Dielectric Core-Shell Nanoparticles. *Nano Lett.* **2011**, *11*, 1374–1378. [CrossRef]

31. Wang, Z.N.; Shi, X.Y.; Wei, S.J.; Sun, Y.Y.; Wang, Y.R.; Zhou, J.; Shi, J.W.; Liu, D.H. Two-threshold silver nanowire-based random laser with different dye concentrations. *Laser Phys. Lett.* **2014**, *11*, 095002. [CrossRef]

32. Perumbilavil, S.; Piccardi, A.; Barboza, R.; Buchnev, O.; Kauranen, M.; Strangi, G.; Assanto, G. Beaming random lasers with soliton control. *Nat. Commun.* **2018**, *9*, 3863. [CrossRef] [PubMed]

33. Kurihara, S.; Hatae, Y.; Yoshioka, T.; Moritsugu, M.; Ogata, T.; Nonaka, T. Photo-tuning of lasing from a dye-doped cholesteric liquid crystals by photoisomerization of a sugar derivative having plural azobenzene groups. *Appl. Phys. Lett.* **2006**, *88*, 103121. [CrossRef]

34. Ziegler, J.; Djiango, M.; Vidal, C.; Hrelescu, C.; Klar, T.A. Gold nanostars for random lasing enhancement. *Opt. Express* **2015**, *23*, 15152. [CrossRef] [PubMed]

35. Sarkar, A.; Subhashree, O.N.N.; Shivakiran, B.B.N. Effect of photonic stop-band on the modes of a weakly scattering DCM-PVA waveguide random laser. *Appl. Phys. Lett.* **2017**, *110*, 251104. [CrossRef]

36. Ye, L.H.; Feng, Y.Y.; Cheng, Z.X.; Wang, C.L.; Lu, C.G.; Lu, Y.Q.; Cui, Y.P. Coherent random lasing from dye aggregates in polydimethylsiloxane thin films. *ACS Appl. Mater. Interfaces* **2017**, *9*, 27232–27238. [CrossRef]

37. Nesrullajev, A.; Avc, N. Oriented and non-oriented textures of nematic liquid crystals: Comparative peculiarities of the thermotropic behavior. *Mater. Chem. Phys.* **2011**, *131*, 455–461. [CrossRef]

38. Ferjani, S.; Barna, V.; De Luca, A.; Versace, C.; Strangi, G. Random lasing in freely suspended dye-doped nematic liquid crystals. *Opt. Lett.* **2008**, *33*, 557–559. [CrossRef]

39. Bian, H.T.; Yao, F.F.; Gao, Y.P.; Pei, Y.B.; Zhang, J.L.; Sun, X.D. Random lasing in unbounded dye-doped nematic liquid crystals. *Liq. Cryst.* **2016**, *43*, 581–586. [CrossRef]

40. Andreasen, J.; Bachelard, N.; Bhaktha, S.B.N.; Cao, H.; Sebbah, P.; Vannsete, C. Partially pumped random lasers. *Int. J. Mod. Phys. B* **2014**, *28*, 1430001. [CrossRef]

41. Leonetti, M.; Conti, C.; Lopez, C. The mode-locking transition of random lasers. *Nat. Photonics* **2011**, *5*, 615. [CrossRef]